Industrial & Engineering Chemistry Research, Volume 64, Issue 29, July 2025, pp. 14616-14627
DOI: 10.1021/acs.iecr.5c01422

Blast furnace gas utilisation with Calcium Assisted Steel-mill Off-gas Hydrogen production (CASOH) technology: Technical evaluation

Navid Khallaghi [a,b], Santiago Zapata-Boada [a], Miriam Diaz Gutierrez [c], Andrew David Wright [a], Jose Ramon Fernandez [c], Juan Carlos Abanades [c], Vincenzo Spallina [a,1]

[a] *Department of Chemical Engineering, University of Manchester, Manchester, United Kingdom*

[b] *Centre for Energy Decarbonisation and Recovery (CEDAR), Cranfield University, Bedford, Bedfordshire, MK43 0AL, UK.*

[C] *CSIC-INCAR, Francisco Pintado Fe, 26, Oviedo, 33011, Spain*

[1] *Corresponding author:* Vincenzo.spallina@manchester.ac.uk

Contents

Table of Contents – Graphics

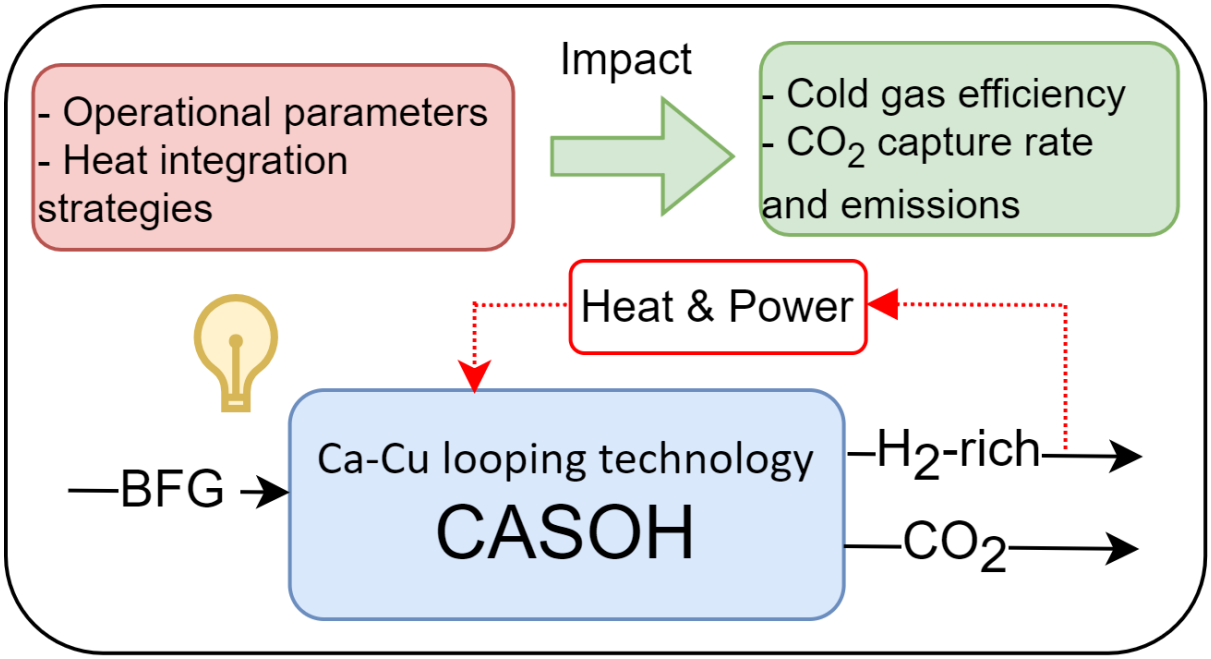

Abstract

In pursuit of decarbonising the iron and steel industry through the utilisation of Blast Furnace Gas (BFG), this study investigates the technical feasibility of a Ca-Cu looping technology known as Calcium-Assisted Steel-mill Off-gas Hydrogen Production (CASOH). The process is modelled and analysed using Aspen Plus software. The key technical performances of two versions of CASOH were evaluated and compared with more traditional solvent-based technology for the pre-combustion decarbonisation of BFG using methyl diethanolamine (MDEA). The first case (base case, CASOH-B) uses part of the BFG to regenerate the sorbent; therefore, it concentrates CO_2 up to 54%. In the second case (enhanced, CASOH-E), low-pressure steam is used for the calcination reaction. In the case of CASOH-B, the integration with a CO_2 purification unit outperforms the other configurations regarding CO_2 capture efficiency, with values up to 97% compared to 91% for CASOH-E and 83% for MDEA. However, CASOH-E demonstrated a significantly higher thermal output (224.5 MW_{LHV} vs. 77.6 MW_{LHV} for CASOH-B), resulting in better cold gas efficiency and lower specific CO_2 emissions (76% and 29.8 kg_{CO2}/GJ_{LHV} for CASOH-E, compared to 26.3% and 105.7 kg_{CO2}/GJ_{LHV} for CASOH-B). Various scenarios were analysed to meet the heat and power requirements of the process. When relying on external energy sources such as natural gas, biogas, or photovoltaic panels, the solvent-based case outperforms the CASOH configurations with a specific energy consumption per CO_2 avoided (SPECCA) of 0.5–0.7 MJ_{LHV}/kg_{CO2}, compared to 1.1–3.3 MJ_{LHV}/kg_{CO2} for CASOH configurations. However, if the hydrogen-rich stream produced in CASOH-E is used to meet energy demands, CASOH-E becomes the most favourable option. These findings emphasise the importance of operational parameters in optimising BFG decarbonisation strategies by balancing thermal output, efficiency, and emissions capture.

Keywords: pre-combustion, iron and steel industry, carbon capture, Ca-Cu looping

70 **List of Abbreviations**

BF-BOF	Blast furnace-basic oxygen furnace
BFG	Blast furnace gas
BOFG	Basic Oxygen Furnace Gas
CASOH	Calcium-assisted steel-mill off-gas hydrogen production
CCR	CO_2 capture rate
CGE	cold gas efficiency
COG	Coke oven Gas
DAC	Direct air capture
DCF	Decarbonised fuel
EAF	Electric arc furnace
MOF	Metal-organic-framework
OEE	Overall energy efficiency
PSA	Pressure swing adsorption
SPECCA	Specific CO_2 emission and specific primary energy consumption for CO_2 avoided
VPSA	Vacuum-pressure swing adsorption
WGS	Water gas shift

71 **Nomenclatures**

$\dot{m}$	Mass flow rate
Q_{th}	Heat requirement
E_{th}	Emissions from heat production
W_{el}	Electricity requirement
E_{el}	Emissions from electricity production

72

73

1. Introduction

The steel industry is widely recognised for its high consumption of energy and greenhouse gas (GHG) emissions, accounting for approximately 7-9% of global anthropogenic CO_2 emissions [1]. The carbon-intensive nature of steel production and increasing global demand pose significant challenges for climate change mitigation efforts.

Steel production primarily relies on two main routes: the integrated blast furnace-basic oxygen furnace (BF-BOF) route and the electric arc furnace (EAF) route. The BF-BOF route, which accounts for about 70% of global steel production [2], is particularly carbon-intensive due to its reliance on coal as a fuel and reducing agent. In this process, iron ore is reduced to pig iron in blast furnaces using coke derived from coal, followed by conversion to steel in basic oxygen furnaces. The EAF route, which primarily uses recycled steel scrap as input, is less carbon-intensive but is limited by scrap availability and quality requirements for certain steel grades [3].

Blast furnace gas (BFG) is a by-product of the ironmaking process in blast furnaces and plays a significant role in the overall emissions profile of integrated steel plants. BFG is generated when hot air is blown into the blast furnace, reacting with coke and other carbon-based materials used in the ironmaking process [4]. The composition of BFG typically includes carbon monoxide (CO) at 20-30%, carbon dioxide (CO_2) at 20-25%, hydrogen (H_2) at 1-5%, nitrogen (N_2) at 50-55%, and small amounts of other gases [4]. While BFG has a low calorific value compared to natural gas (about 3-4 MJ/Nm^3 versus 35-40 MJ/Nm^3 for natural gas), it is produced in large quantities and is commonly used as a fuel within the steel plant. This internal use of BFG helps to reduce the overall energy consumption of the steelmaking process, but it also represents a significant source of CO_2 emissions when combusted [5]. Therefore, developing strategies to either reduce BFG generation, capture its CO_2 content, or find alternative uses for BFG are crucial aspects of steel industry decarbonisation efforts [6].

Chemical looping is an advanced technology used primarily for energy production and carbon capture. Chemical looping uses a solid oxygen carrier, typically a metal oxide, to transfer oxygen from air to fuel, avoiding direct contact between fuel and air and facilitating easier CO_2 capture [7]. This technology involves both exothermic (i.e., oxidation of the metal oxide) and endothermic (i.e., reduction of the metal oxide with fuel) reactions. The combination of these reactions can result in an overall exothermic process due to the heat released during the oxidation step [8]. Recent research has demonstrated the feasibility of chemical looping for BFG treatment at laboratory and pilot scales [9]. Calcium looping has been extensively investigated for its potential in post-combustion CO_2 capture from power plants, biomass-fuelled technologies, and recently for Direct Air Capture (DAC) [10-12] and also as a method for BFG decarbonisation [7]. Moreover, calcium looping has been suggested as

a viable approach for hydrogen production in reforming processes, exhibiting notable benefits such as high CH_4 conversion and hydrogen purity, all achieved at temperatures below 650°C [13, 14]. However, the primary limitation of this technology resides in the cost associated with regenerating $CaCO_3$, a process requiring temperatures above 850°C and either the presence of pure oxygen from an Air Separation Unit [10, 15] or the utilisation of thermal storage to transfer heat from the carbonator to the calciner [16]. Consequently, addressing the economic and energy-intensive nature of $CaCO_3$ regeneration is imperative to successfully implementing calcium looping technology.

A potential alternative lies in integrating chemical and calcium looping, utilising a copper-based oxygen carrier (OC). Abanades et al. [17] proposed combining the calcium-copper (Ca-Cu) looping process to offset the energy requirements of calcination through the exothermic reduction of CuO with gaseous fuel by combining the reactions (R1-R6) to facilitate the CO_2 capture from the treated fuel.

$$CO_2 + CaO \leftrightarrow CaCO_3 \qquad \Delta H^0_{298\,K} = -178.8\ \mathrm{kJ/mol_{CO_2}} \qquad \text{(R1)}$$

$$CaCO_3 \leftrightarrow CO_2 + CaO \qquad \Delta H^0_{298\,K} = 178.8\ \mathrm{kJ/mol_{CO_2}} \qquad \text{(R2)}$$

$$CO + H_2O \leftrightarrow CO_2 + H_2 \qquad \Delta H^0_{298\,K} = -41.2\ \mathrm{kJ/mol_{CO}} \qquad \text{(R3)}$$

$$CO + CuO \rightarrow CO_2 + Cu \qquad \Delta H^0_{298\,K} = -127.8\ \mathrm{kJ/mol_{CO}} \qquad \text{(R4)}$$

$$H_2 + CuO \rightarrow H_2O + Cu \qquad \Delta H^0_{298\,K} = -86.6\ \mathrm{kJ/mol_{H_2}} \qquad \text{(R5)}$$

$$O_2 + Cu \rightarrow CuO \qquad \Delta H^0_{298\,K} = -310.4\ \mathrm{kJ/mol_{O_2}} \qquad \text{(R6)}$$

Alarcon et al.[18] demonstrated the feasibility of this process using commercially available materials. Later, Fernández et al. [7] expanded its application to the decarbonisation of blast furnace gas (CASOH process). More recently, Abbas et al.[19, 20] have experimentally shown that the CASOH process is a viable alternative not only for decarbonising BFG but also for producing an H_2-rich gas. However, the CASOH process exhibits two significant drawbacks that hinder its overall performance. Firstly, only 1/3rd of the BFG is utilised for hydrogen production [21]. Secondly, owing to the high N_2 content in the BFG, a CO_2 purification process is required on the CO_2-rich stream [22].

Hence, this study proposes integrating the CASOH technology with downstream purification via adsorption and low-temperature condensation to achieve high CO_2 purity. In addition, it proposes a new layout of the process, called CASOH-enhanced. Moreover, it is compared with the pre-combustion process using MDEA, which was previously evaluated as benchmark [23]. Different CO_2 purification systems based on CO_2 partial condensation, pressure swing adsorption and hybrid scenarios are modelled and integrated into the CASOH-base to reach the required CO_2 purity for storage. Then, a comprehensive comparison is carried out among the abovementioned cases

regarding fuel conversion (cold gas efficiency), specific CO_2 emission and specific primary energy consumption for CO_2 avoided (SPECCA). Finally, a sensitivity analysis is performed on CASOH-enhanced with different capture rates and calcination pressures.

2. Methodology

Process simulations of the CASOH-Base and CASOH-Enhanced are conducted using Aspen Plus® software v12.1, assuming a BFG flow rate of 3.5×10^6 tonnes per year [1, 24]. This flow rate allows for a realistic evaluation of the proposed configurations in the context of an actual steelmaking facility. The following sections describe the modelling approach of the benchmark (MDEA), CASOH-B, and CASOH-E processes.

2.1. MDEA CO_2 capture unit (Benchmark)

Figure 1 shows the schematic of the benchmark technology, which has been evaluated in Khallaghi et al. [23] and here briefly introduced. In this process, BFG from the steel mill is mixed with steam to attain an H_2O/CO ratio of 1.5. The resulting mixture is then heated to 330˚C and introduced into the WGS reactor to generate a syngas through a single-stage water gas shift (WGS) reaction. It is cooled down by pre-heating the inlet gases and subsequently brought to ambient temperature before entering the absorber column. In the absorber column, the syngas undergoes counter-current contact with the MDEA solvent, leading to the removal of CO_2. The high-purity CO_2 stream obtained from the stripper unit is directed to the compression unit, where it undergoes pressurisation to 78 bar using a multi-stage compressor with inter-stage cooling. The CO_2 is then liquified by cooling to 25˚C and pumped to the final delivery pressure of 110 bar. Finally, decarbonised syngas is obtained, with a mass flowrate of 75.9 kg/s and a composition of 24.0% H_2, 61.8% N_2, 6.4% CO, 2.3% CO_2 and 5.5% H_2O.

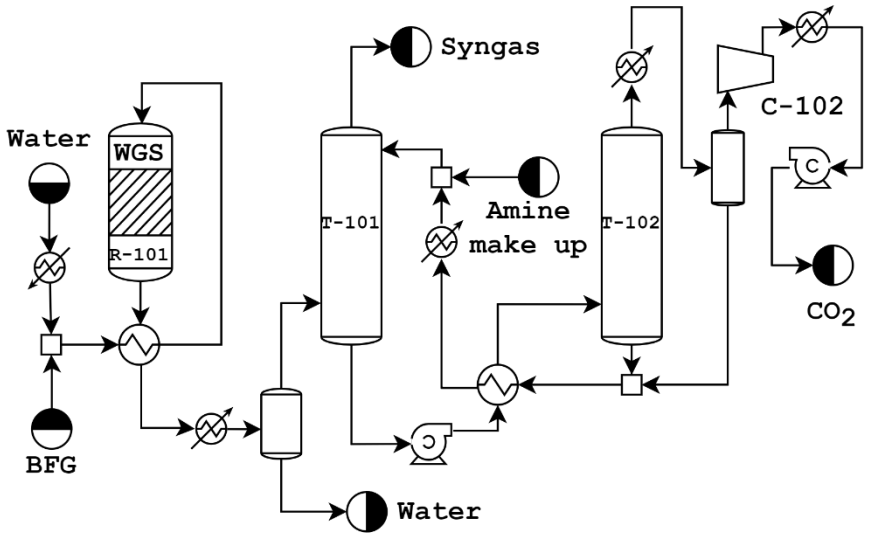

154

155 **Figure 1**. MDEA CO_2 capture unit (Reproduced from ref [23]. Available under a CC-BY 4.0 license.
156 Copyright Elsevier, Khallaghi et al.[23]

157 ### 2.2. Calcium Assisted Steel-mill Off-gas Hydrogen: CASOH-Base (CASOH-B)

158 Figure 2 shows the schematic of the CASOH base case (CASOH-B). It comprises three primary steps:
159 CASOH reaction, oxidation, and regeneration. During the CASOH step, a fraction of the BFG
160 (approximately 1/3 of the total flow rate) is compressed to 10 bar and combined with steam before
161 entering the CASOH reactor. The remaining BFG fraction is directed to the regeneration stage. The
162 split between BFG to CASOH and to regeneration is dictated by the reactor thermal management since
163 the appropriate solid temperature is needed during regeneration. Within the CASOH reactor, the CO
164 in the BFG is converted into CO_2 and H_2 through the calcium-assisted WGS reaction (R3), utilising a
165 steam-to-CO ratio of 1.2. Concurrently, a carbonation reaction (R1) occurs between the CaO sorbent
166 and the CO_2 generated by the WGS reaction and the initial CO_2 present in the BFG. This carbonation
167 reaction facilitates the formation of $CaCO_3$ and enhances the conversion of CO by shifting the
168 equilibrium towards increased production of CO_2. The Cu-based particles in the reactor bed act as
169 catalysts in this stage, facilitating the WGS reaction and promoting the production of hydrogen-rich
170 syngas.

171 After the CASOH reaction, the process enters the oxidation stage. In this step, air is introduced into
172 the reactor to convert Cu into CuO, generating oxygen-depleted air (reaction R6). This step is
173 conducted at high pressure (10 bar) and moderate temperature (765 °C) to minimise CO_2 slip from
174 partial calcination of $CaCO_3$.

175 In the subsequent regeneration step, the remaining fraction of BFG (roughly two-thirds of the total
176 flow) is used to restore the reaction conditions and recover the sorbent material. The calcination

reaction (R2) thermally decomposes $CaCO_3$ back into CO_2 and CaO. To provide the necessary heat, BFG reacts with CuO to reduce it back to metallic Cu, following reactions R4 and R5. These reduction reactions contribute to catalyst regeneration and lead to additional CO_2 and H_2O, which, together with nitrogen in the BFG, form a product gas that is later cooled to condense water vapour. The simultaneous occurrence of redox and calcination reactions within the solid bed eliminates the need for an external heat source to meet the energy requirement of the calcination process. To facilitate $CaCO_3$ decomposition, the reaction is carried out at low pressure (atmospheric). In practice, this is achieved through cyclic operation of multiple fixed-bed pressure swing reactors, where each unit undergoes different stages at specified pressures and temperatures.

A heat removal step is implemented to control the temperature and the extent of each reaction stage. Heat removal is carried out using an inert gas (e.g., N_2 obtained in the oxidation step), which circulates in a semi-closed-loop system to absorb and remove excess heat, thereby harnessing high-temperature energy for further utilisation [7] like steam generation or power production which is credited toward the system's overall energy efficiency which will be discussed later.

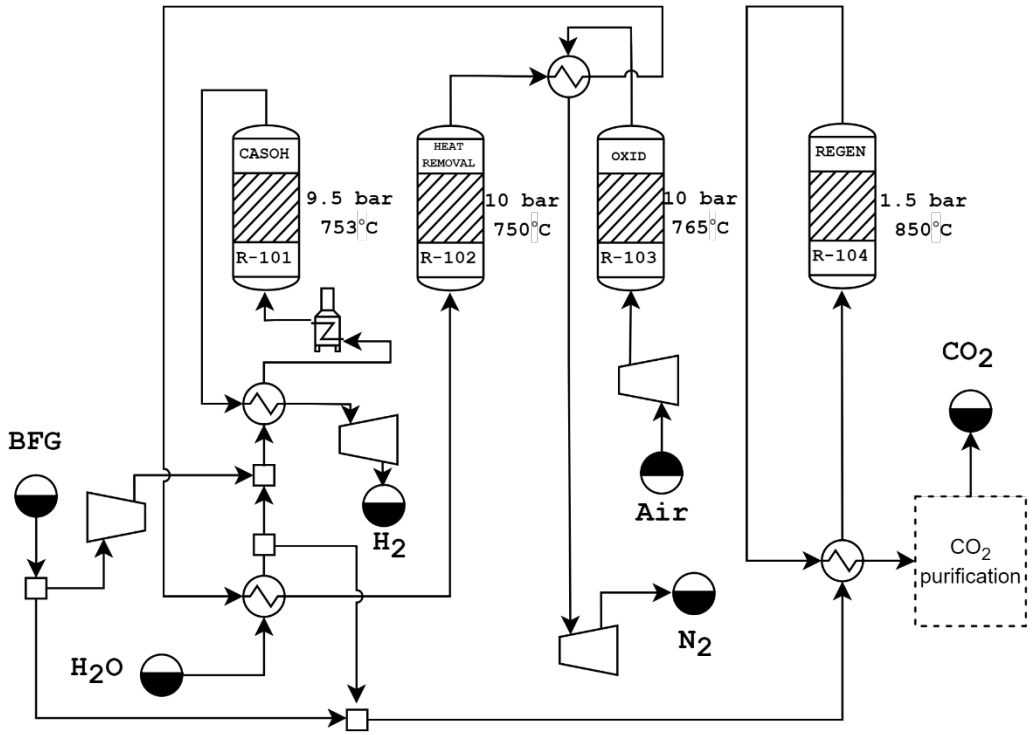

Figure 2. Schematic of CASOH-Base

The CASOH process described above was modelled following Grasa et al.[25] and Diaz et al.[26], who developed a one-dimensional pseudo-homogeneous fixed-bed reactor model to simulate the interplay of reaction kinetics, mass transfer, and heat dynamics across all three stages (CASOH,

oxidation, and regeneration). The model integrates axial mass and energy balances with dispersion effects, accounting for key reactions such as the calcium-assisted water-gas shift (R3), CaO carbonation (R1), Cu oxidation (R6), and CuO reduction coupled with $CaCO_3$ calcination (R2, R4–R5). Kinetic parameters for these reactions, derived experimentally from fixed-bed tests and thermogravimetric analyses [25], were incorporated. Experimental demonstration of the key CASOH reaction steps has recently been achieved in a TRL7 pilot treating BFG from the ArcelorMittal factory in Spain [27]. Numerical solutions of the 1D packed bed reactor model (described in detail in previous works [25, 26] were obtained using MATLAB to predict gas compositions, temperature profiles, and solid conversions. These operational parameters were implemented in the Aspen Plus simulation of the CASOH process, described in section 2.4.

The CO_2-rich stream after the regeneration step contains N_2, which is present in the BFG gas used at the inlet (>45% vol.). To achieve the CO_2 quality for transportation and storage, an additional purification step is needed to remove the excessive N_2. The following section describes different purification strategies assessed in this study.

2.2.1. CO_2 separation by partial condensation

The CO_2-rich purification via multistage partial condensation has been described in Khallaghi et al. [22]. The CO_2-rich stream from the regeneration phase is subjected to compression through a multi-stage compressor, leading to a pressure of 25 bar, and subsequently cooled to -49°C in a cold box regeneration unit. Then, the stream is introduced into the initial flash separator to recover part of the CO_2 in the liquid phase. Subsequently, the resulting vapour undergoes further cooling to -51°C before being directed into the second flash separator, where additional CO_2 is partially recovered. This vapour stream is compressed to 60 bar, and further temperature reduction to -55°C is achieved using a refrigeration system. The pressure and temperature for CO_2 condensation are considered to avoid the freezing point of CO_2. After cooling, the cold stream is channelled into a third flash vessel to facilitate additional CO_2 recovery. An extra flash separator is employed to enhance the purity of the recovered CO_2. Finally, the CO_2 is pressurised to 110 bar. Heat recovery is carefully considered to reduce the unit's refrigeration cost. More details on the partial condensation process are found in [22].

2.2.2. CO_2 separation by vacuum-pressure swing adsorption (VPSA)

A vacuum-pressure swing adsorption process is proposed as an alternative to the partial condensation route. Metal organic framework (MOF) adsorbent IISERP MOF2, which proved most effective in the work of Subraveti et al. [28], was selected in this application. Yet, due to the water sensitivity of IISERP MOF2, it is assumed that the gas stream entering the VPSA unit is pre-dried using standard flue gas

conditioning techniques such as condensation, desiccant drying, or molecular sieves. This ensures the adsorbent's structural stability and does not materially affect the process's feasibility.

The CO_2 VPSA was simulated using a proprietary and purpose-built model written in C++. Therefore Aspen Plus was not used for calculating the energy/power requirements for this particular unit nor for obtaining the material balance. Instead, a separate piece of software was used to perform the dynamic simulations and the time-average results were fed back into the Aspen Plus model.

The cycle employed requires 7 vessels, each containing 108,000 kg of adsorbent. Three of these are on feed at any time, with 2 undergoing vacuum extraction to obtain the CO_2 product gas. Each of the 7 vessels goes through an adsorption cycle that starts with a feed step in which compressed CO_2-rich gas feed is passed through an adsorbent vessel, and a CO_2-depleted gas stream is obtained, throttled down to atmospheric pressure and vented. Once the adsorbent vessel is filled with CO_2, an equalisation step occurs, where the gas pressure is reduced by transferring the contents to another vessel in the system. This partially depressurised vessel is then held in an idle state before being vacuumed out in the counter-current direction to remove the adsorbed CO_2. Following the vessel's evacuation, the pressure is brought back up to that of the vessels on feed. The total cycle time is of around 280 seconds, at which point all the steps are repeated in a cyclic manner. The design target was 90 % recovery of the CO_2 from the feed gas with no more than 3 % impurities in the CO_2 product. This is a higher purity specification than normally seen in designs for CO_2 VPSA units (typically 5 %). However, this was chosen to allow margin for feed gas leaking into the product gas through the valves, which can be quite large at this scale. The optimum feed pressure to minimise overall power consumption was 3 bar, with the vacuum step taking the vessel pressure down to 0.4 bar. The CO_2 product gas is compressed to 1.4 bar using a vacuum pump and fed into a buffer tank, which is needed to allow a constant flow rate to be fed to the compressor. The pressure in the buffer tank varies between 1.4 bar and 1.1 bar and discharges to a CO_2 compressor running with a constant molar inlet flow rate at 1 bar [28]. The CO_2 compressor increases the pressure of the gas to 78 bar, after which it is liquified at 25 °C and pumped to 110 bar.

2.2.3. CO_2 separation by VPSA and partial condensation

A problem with the previous design is that the chosen MOF material is costly and still in development. It is also water sensitive; therefore, pre-drying the gas stream is required, which adds additional operating and capital costs. Thus, as an alternative, the VPSA was redesigned using HZSM-5, a commercially available material at a lower price. However, it has a lower capacity and selectivity than IISERP MOF2, which makes designing the VPSA to meet the required purity and recovery specifications quite difficult. The VPSA was designed to capture 90% of the CO_2 at a purity of 87%. This was optimised

at an adsorbent mass per vessel of 197,000 kg and running with a feed pressure of 2 bar and a vacuum pressure of 0.23 bar. The purity of the CO_2 product gas from the VPSA was increased to 97% (standard specification for pipeline transport and geological storage) [29] by processing it through a partial condensation process requiring fewer separation flashes than that by partial condensation alone. The N_2-rich off-gas from the partial condensation unit is recycled back to the feed of the VPSA to maintain the required CO_2 capture rate.

2.2.4. CO_2 separation by partial condensation and pressure swing adsorption (PSA)

A partial condensation unit is used to produce CO_2 directly from the CO_2/N_2 feed gas mixture. However, the low purity of CO_2 in the feed gas results in a low recovery of CO_2. Therefore, a PSA unit is used to capture the CO_2 from the N_2-rich gas leaving the partial condensation unit. The chosen adsorbent is silica gel, which was simulated using data obtained from Guan et al. [30]. As this PSA operates at a much higher pressure than for the VPSA cases, the amount of adsorbent required reduces significantly to 46,000 kg per vessel. Silica gel is also a commercial material available at a considerably lower price than IISERP MOF2 or HZSM-5. The process is designed to achieve a net 90 % capture rate from the feed gas. This was achieved with only 6% of the N_2 passing through being co-adsorbed and recycled back to the feed stream, which compares with 8% using a membrane, as reported in White and Allam [31].

2.3. Calcium Assisted Steel-mill Off-gas Hydrogen: CASOH-Enhanced (CASOH-E)

Figure 3 shows the schematic of the CASOH-E process, which comprises four primary steps: CASOH-reaction, calcination, oxidation, and reduction. In the first step, the sorption-enhanced conversion of BFG into H_2-rich syngas occurs with the same principle as the base case, and all BFG is processed at high pressure (10 bar), increasing the amount of BFG converted into an H_2-rich product. The exothermic reactions of carbonation (R1) and WGS (R3) raise the temperature of the reactor bed to 749.5 °C. The Cu inside the bed behaves as a WGS catalyst since it is reduced. In the calcination step, the bed is depressurised under mild vacuum conditions (0.5 bar), and high-temperature H_2O is introduced to further reduce CO_2 partial pressure. This causes a sudden change in the partial pressure of CO_2 in the solid bed, which promotes the decomposition of $CaCO_3$ into CaO and high-purity CO_2 (R2). The heat previously accumulated in the reactor during the CASOH stage is used for the endothermic regeneration of the sorbent, causing an adiabatic cooling of the solids until reaching a temperature of 785 °C [32]. At this point, most of the heat generated from the carbonation is removed via calcination; however, some heat inside the bed needs to be removed. This is possible by feeding N_2 at 600 °C, and the heat generated is then used to provide part of the gas heating and steam generation. The maximum feeding temperature of the N_2 is limited by the materials of the boosters

and upstream heat exchanges; therefore, to have an optimal solid temperature before the new cycle starts, oxidation (R6) and reduction with H_2 (R5) steps are required. In summary, four main differences can be highlighted with the CASOH-B scheme:

1) The mild vacuum calcination step facilitates the production of a sufficiently pure CO_2 stream, avoiding the need for an extra purification system.
2) Only 15% of the H_2-rich gas is needed for the CO_2-free reduction step, while the remaining gas is available as a product.
3) The heat removal stage requires less N_2 flowrate, reducing the high-temperature heat generation in the process.
4) The system requires additional thermal utilities to generate the steam needed for the calcination.

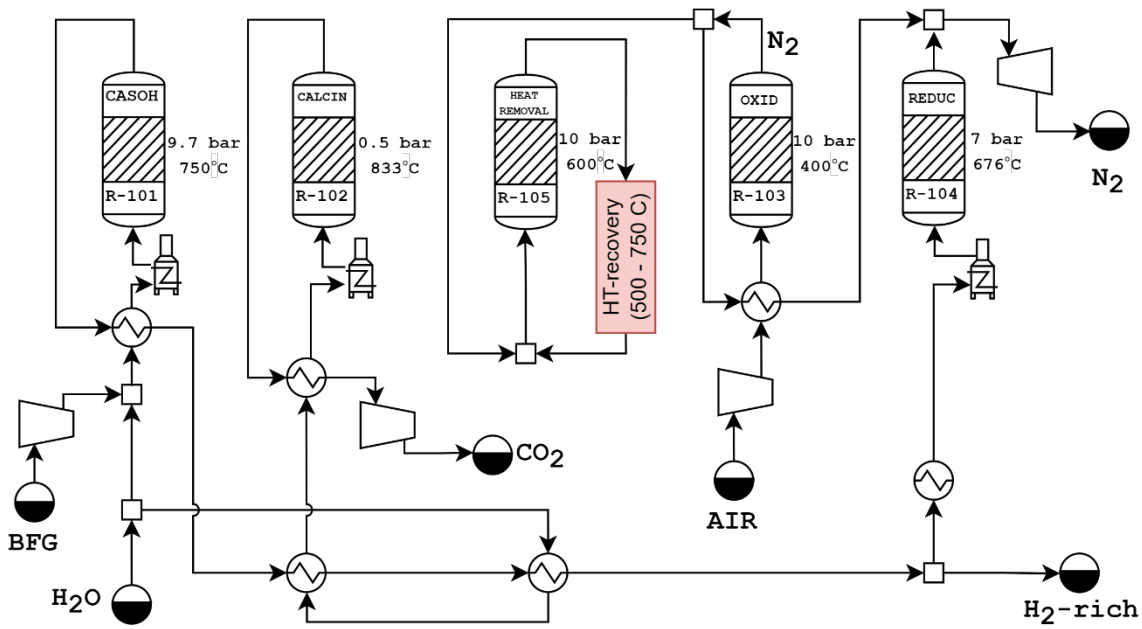

Figure 3. Schematic of CASOH-Enhanced

2.4. Model development

Table 1 summarises the parameters used in Aspen Plus for different components. Since the process is dynamically operated, the simulation in Aspen Plus relies on the averaged conditions at each reactor outlet, which have been determined by the rigorous reactor model simulation following Grasa et al. [25] and Diaz et al.[26].

While pressure is manipulated assuming that the valves and compressor could control the operating conditions, the temperature indicated is the average temperature (over the cycle time) at each reactor outlet stage and it is not fixed but determined by the extent of the reaction/heat fronts, cycle time

316 and gas feeding. These values have been calculated using an in-house reactor model. More
317 specifically:
318 In CASOH-B, the oxidation occurs after the carbonation (CASOH) and 1st heat removal and being
319 oxidation highly exothermic, high pressure and limited maximum temperature of the bed are required
320 for to avoid CO_2 decomposition and losses with the O_2-depleted air because of the
321 carbonation/calcination equilibrium (R1 and R2). The reduction occurs at the same time than
322 calcination and it is required to generate energy at high temperature (and low pressure) to
323 compensate for the endothermic reaction of calcination.
324 In CASOH-E, oxidation and reduction occur after the calcination (that occurs at low pressure) and heat
325 removal they are required to condition the solid ed temperature for the following carbonation
326 reaction. Since the reactor does not contain CO_2 (ad $CaCO_3$), there is no need to control the calcination
327 reaction and therefore oxidation and reduction pressure are defined from upstream processes based
328 on compressor operating conditions.
329

330 **Table 1.** Process modelling of CASOH-B and CASOH-E providing operating pressure and final time-
331 averaged temperature at the outlet.

Reactors	Scenario	
	CASOH-B	**CASOH-E**
CASOH	9.5 bar, 753˚C, 99% CO conversion	9.7 bar, 750˚C, 99% CO conversion
Heat removal	10 bar, 750˚C	10 bar, 600˚C
Calcination	-	0.5 bar, 833˚C
Oxidation	10 bar, 765˚C	10 bar, 400˚C
Reduction	1 bar, 850˚C	7 bar, 676˚C

332 VPSA was designed similarly to that suggested by Subraveti et al. [28] with minor modifications to the
333 process cycle. For VPSA and PC, the VPSA was designed as described by Masala et al. [33], while the
334 partial condensation process was described by White and Allam [31]. For the PC and PSA, a similar
335 partial condensation process was described by White and Allam [31], which uses a membrane on the
336 N_2-rich off-gas to enable a higher recovery of CO_2. In this work, the membrane was replaced by a 10-
337 bed PSA unit operating in the same manner as for the H_2 PSA described in Argyris et al. [34]. Table 2
338 reports the list of assumptions used to simulate the process units.

339 **Table 2.** Assumptions and initial inputs for simulation

Parameters	Value
Heat Exchangers (high temperature)	
Min △T gas-gas, °C	25
Min △T gas-liq, °C	10
Min △T liq-liq, °C	10
Min △T for partial condensation heat exchangers	2
Pressure drops, % bar	2

Compressors	
Isentropic efficiency, %	85
Mechanical-electrical efficiency, %	95
Expanders	
Isentropic efficiency, %	93
Mechanical-electrical efficiency, %	99

2.5. Thermodynamic evaluation indicators

The system's thermodynamic performance is measured using cold gas efficiency (*CGE*), which relates the thermal energy output to the thermal energy input, as per Equation (1). This metric provides insights into the system's efficiency in converting the input energy from BFG into the desired output of the H_2-rich stream.

$$\mathrm{CGE} = \frac{\dot{\mathrm{m}}_{\mathrm{H_2-rich}} \times \mathrm{LHV}_{\mathrm{H_2-rich}}}{\dot{\mathrm{m}}_{\mathrm{BFG}} \times \mathrm{LHV}_{\mathrm{BFG}}} \quad (1)$$

The CO_2 specific emissions (E_{CO2}) are calculated by Equation (2) and quantify the amount of CO_2 emitted per unit of product (H_2-rich stream) generated.

$$\mathrm{E}_{\mathrm{CO_2}}\left[\frac{\mathrm{kg}_{\mathrm{CO_2}}}{\mathrm{GJ}_{\mathrm{LHV,H_2-rich}}}\right] = \frac{\dot{\mathrm{m}}_{\mathrm{CO2,captured}}}{\dot{\mathrm{m}}_{\mathrm{H_2-rich}} \times \mathrm{LHV}_{\mathrm{H_2-rich}}} \quad (2)$$

The equivalent CO_2 specific emissions ($E_{CO2,eq}$) are calculated by Equation (3) based on CO_2 vented to the atmosphere and the equivalent emissions associated with electricity (E_{el}) and heat (E_{th}) requirement (Table 3).

$$\mathrm{E}_{\mathrm{CO_2,eq}}\left[\frac{\mathrm{kg}_{\mathrm{CO_2}}}{\mathrm{GJ}_{\mathrm{LHV,LF}}}\right] = \frac{\dot{\mathrm{m}}_{\mathrm{CO_2,emitted}} + \mathrm{Q}_{\mathrm{th}} \times \mathrm{E}_{\mathrm{th}} + \mathrm{W}_{\mathrm{el}} \times \mathrm{E}_{\mathrm{el}}}{\dot{\mathrm{m}}_{\mathrm{H_2-rich}} \times \mathrm{LHV}_{\mathrm{H_2-rich}}} \quad (3)$$

Table 3. Considered emissions associated with different energy production technologies [35-37]

	Unit	Value
Electricity from grid	[kg_{CO2}/MW_h]	529
Natural gas combined cycle	[kg_{CO2}/GJ_{el}]	127.2
Natural gas boiler	[kg_{CO2}/GJ_{th}]	105.8
Biogas combined cycle	[kg_{CO2}/GJ_{el}]	84.4
Biogas boiler	[kg_{CO2}/GJ_{th}]	84.4
Photovoltaic solar panel	[kg_{CO2}/GJ_{el}]	21.7

CO_2 capture rate (*CCR*), calculated by Equation (4), represents the percentage of CO_2 that is successfully captured and stored. *CCR* is calculated assuming that all BFG carbon content is converted into CO_2. Finally, SPECCA is obtained with Equation (5), and it quantifies the energy required to avoid one unit of CO_2 emission during the process.

$$\mathrm{CCR}[\%] = \frac{\dot{m}_{\mathrm{CO2,captured}}}{\dot{m}_{\mathrm{CO2,BFG}}} \quad (4)$$

$$\mathrm{SPECCA}\left[\frac{\mathrm{MJ_{LHV}}}{\mathrm{kg_{CO2}}}\right] = \frac{\left(\frac{1}{\mathrm{OEE_{Captured}}} - \frac{1}{\mathrm{OEE_{no\ capture}}}\right)}{\mathrm{E_{CO2,no\ capture}} - \mathrm{E_{CO2,captured}}} \quad (5)$$

356

357 ## 3. Results and discussion

358 ### 3.1. Mass and energy balance comparison

359 The comparison of the thermodynamic performance of the CASOH-B, CASOH-E and MDEA processes
360 is presented in Table 4. In all cases, the thermal input (energy content of the BFG) is 295.2 MW. The
361 complete PFD and stream tables of the CASOH-B, CASOH-E, and MDEA processes are presented in the
362 Supplementary Material.

363 **Table 4.** Comparison of the thermodynamic performance of the CASOH-B, CASOH-E and MDEA cases

	CASOH-B					CASOH-E	MDEA
	No purif.	**PC**	**VPSA**	**VPSA+PC**	**PC+PSA**		
Thermal energy output [MW]	77.6	77.6	77.6	77.6	77.6	224.5	267.4
Cold gas efficiency [%]	26.3	26.3	26.3	26.3	26.3	76.1	90.6
Power requirement [MWel]	4.9	44.5	49.2	54.9	47.1	75.2	33.6
Required heat [MWth]	-136	-136	-136	-136	-136	57.4	142.6
CO_2 flow rate for storage [kg/s]	78.2	62.6	70.6	70.6	71	72.5	66.4
CO_2 purity for storage [%]	53.9	97.2	97.1	97.3	96.2	99.8	98.2
CO_2 emission (direct**) [kg/s]	1	16.6	8.6	8.6	8.2	6.7	13.4
CCR [%]	*	79	89.1	89.1	89.6	91.5	83.1
Specific CO_2 emission [$kgCO_2/GJ_{LHV}$]	*	213.9	110.8	110.8	105.7	29.8	50.1

*Although CO_2 is separated, the resulting stream has a purity of 53.9% and is unsuitable for storage. Therefore, it is not counted as captured CO_2, and CCR and specific CO_2 emissions are not reported for this case

** Direct refers to the CO_2 emission from the process only and doesn't account for the emission associated with the energy supply.

364 The thermodynamic performance of the CASOH-B case using different CO_2 separation technologies is
365 detailed in Table 4. In all cases, a thermal output (expressed as H_2-rich gas LHV) of 77.6 MW_{th} is
366 attained, as only one-third of the BFG enters the CASOH reactor, contributing to H_2-rich gas
367 production. Consequently, the cold gas efficiency for all cases is 26.3%. The primary work requirement
368 stems from CO_2 purification and compression for storage. As a result, the CASOH-B without a
369 purification unit has significantly lower work requirement (4.9 MW_{el}) compared to the CASOH-B with
370 partial condensation alone (44.5 MW_{el}), VPSA using IISERP MOF2 (49.2 MW_{el}), VPSA using HZSM-5 and

partial condensation (54.9 MW_{el}) and a partial condensation unit with the PSA on the N_2-rich gas (47.1 MW_{el}). The total power requirement using partial condensation with PSA was found to be smaller than using either of the VPSA options, with less adsorbent and notably smaller vessels and footprint.

Within the CASOH reactor, 20.3 kg/s of steam is needed to facilitate the WGS reaction and achieve a steam-to-CO ratio of 1.2, which requires an overall 70.6 MW_{th} of heat at high temperature. However, substantial BFG (2/3 of the total feed) contributes to high-temperature heat production, leading to a net heat recovery of 135.9 MW_{th} (46 MW_{th} medium-grade and 89.9 MW_{th} high-grade heat). While inert gas circulation provides a thermodynamically viable means of heat removal in CASOH-B, practical implementation at an industrial scale involves challenges, especially for medium-grade heat recovery. These include limitations in heat exchanger design due to the low heat capacity of gases, large surface area requirements, and flow stability. In steel plant settings, additional constraints such as limited space and integration with existing heat recovery networks may reduce the effectiveness or feasibility of inert gas-based heat recovery. These aspects should be addressed in future integration studies.

Integrating a purification unit enhances the captured CO_2 purity from 53.9% to 97.2% for the partial condensation, to 97.1% for VPSA using IISERP MOF2, to 97.3% for VPSA using HZSM-5 and partial condensation and to 96.2% for the partial condensation unit with the PSA on the N_2-rich gas. Although the capture efficiency of the CASOH-B with different purification units (79% to 89.6% respectively) is competitive with the MDEA case with 83%, the lower thermal output associated with the CASOH-B results in a significantly higher specific CO_2 emission compared to the MDEA case (105.7- 213.9 kg_{CO2}/GJ_{LHV} vs 50.1 kg_{CO2}/GJ_{LHV}). In addition to energy and purity performance, the scalability of VPSA and PSA purification options is also an important consideration. Both technologies are well-established for industrial gas separation; however, their deployment at a large scale introduces engineering challenges. In the CASOH-B configuration, the gas stream fed to VPSA or PSA is a CO_2-rich flue gas composed primarily of CO_2 and N_2, requiring large adsorbent beds to handle the volume and maintain separation performance. As system size increases, the need for precise cycle timing and valve sequencing becomes more demanding. For VPSA specifically, vacuum generation efficiency decreases at scale, potentially impacting operational costs. These factors indicate that modular design and careful integration will be necessary for industrial-scale application of adsorption-based purification in CASOH-B.

The thermal output of the CASOH-E (expressed as H_2-rich gas LHV) significantly increases compared to the CASOH-B (224.5 MW_{th} and 77.6 MW_{th}), as shown in Table 4. This occurs because all the BFG contributes to producing an H_2-rich gas. In contrast, only a minor fraction (approximately 15%) of the H_2-rich stream is directed towards regeneration. Overall, 57.4 MW_{th} of heat is required for steam

production at the CASOH and calcination stages. CO_2 compression is the plant's primary power demand. The CASOH-E demands a higher net power requirement than the MDEA (75.2 MW_{el} and 33.6 MW_{el}, respectively) due to the higher CO_2 capture efficiency (91.5% and 83.1%, respectively), along with lower calcination pressure (0.5 bar), as opposed to the stripper pressure (6 bar) in the MDEA case. The specific CO_2 emission for CASOH-E demonstrates a substantial reduction compared to the CASOH-B (29.8 and 105.7 kg_{CO2}/GJ_{LHV}, respectively), owing to the higher capture efficiency and thermal output achieved in CASOH-E.

Regarding the MDEA case, the H_2-rich gas generates a thermal output of 267.4 MW, resulting in a cold gas efficiency of 90.6%. The liquefaction process requires 33.6 MW_{el} of power for CO_2 compression for storage. A heat requirement of 142.6 MW_{th} is associated with the boiler heat duty for regeneration (91.5 MW_{el}) and steam production for the WGS process (66.5 MW_{el}). It is worth mentioning that a heat recovery of 15.3 MW_{th} is achievable from cooling the shifted gas stream before entering the absorber column. By employing BFG pre-combustion with MDEA, a CO_2 flowrate of 66.4 kg/s is achieved with a purity of 98.2%. This results in a carbon capture rate of 83.1% and specific CO_2 emission of 50.1 $kg_{CO2}/GJ_{LHV.}$

3.2. Comparison of different scenarios for utility supply

This analysis aims to evaluate the performance of CASOH-B (with CO_2 purification using PC+PSA), CASOH-E, and MDEA cases under five scenarios for utility supply (electricity and heat).

(1) Heat sourced from burning part of the H_2-rich gas, and electricity supplied from the grid (HY-GRID).
(2) Heat sourced from burning part of the H_2-rich gas, and electricity generated by a hydrogen-fired combined cycle (HY-HY).
(3) Heat sourced from natural gas, and electricity generated by a natural gas-fired combined cycle (NG-NG).
(4) Heat sourced from natural gas, and electricity generated by photovoltaic systems (NG-REN).
(5) Heat is sourced from biogas, and electricity is generated by photovoltaic systems (REN-REN).

It is worth mentioning that the energy supply scenarios were developed to represent a range of boundary conditions rather than specific regional contexts. They reflect hypothetical but plausible configurations ranging from fossil-dominant to fully renewable supply, enabling assessment of the capture systems' sensitivity to energy carbon intensity and integration strategy. The CO_2 emission accounting in this study is limited to direct process emissions and indirect energy-related emissions. Embedded emissions from equipment, adsorbent manufacturing, and plant construction are not

considered here. A full life cycle assessment is being conducted by another partner within the project consortium, which will complement this work. Moreover, all the heat and electricity requirements are assumed to be met internally within the plant using specified on-site technologies; therefore, the emissions associated with energy supply are included within the process boundaries. The comparison of the utility supply scenarios is presented in Table *5*, and each scenario is evaluated in the following sections. In all cases, the thermal input is 295.2 MW.

Scenario 1 (HY-GRID): Providing heat from the H_2-rich gas lowers the thermal output for MDEA (from 267.4 MW_{th} to 108.9 MW_{th}) and CASOH-E (from 224.5 MW_{th} to 160.7 MW_{th}), except for the CASOH-B, where no heat duty is needed due to 135.9 MW_{th} of heat generated (see Table 4). The thermal output leads to a decline in the cold gas efficiency for MDEA (90.6% to 36.9%) and CASOH-E (76.0% to 54.4%). Assuming that the high-grade heat recovered in the CASOH-B is used to generate electricity with an efficiency of 40% [38], the power requirement of the CASOH-B reduces significantly from 47.1 MW_{el} to 11.1 MW_{el}. Furthermore, there is still 46.0 MW_{th} recovered heat available, which can be used within the steel plant or sold for other purposes, eliminating the need for additional CO_2 emissions for heat production and compensating the CO_2 emission by heat-related purposes by -5.8 kg/s. The resulting total CO_2 specific emissions (direct and indirect because of the electricity from the grid) for the MDEA case is 168.4 kg_{CO2}/GJ_{LHV} compared to 51.4 kg_{CO2}/GJ_{LHV} and 110.6 kg_{CO2}/GJ_{LHV} for CASOH-B and CASOH-E, respectively. As Table 5 shows, CO_2 emissions from electricity production lower the carbon capture rate for the MDEA and CASOH-E. In contrast, the carbon capture rate for CASOH-B improved from 79% to 95% due to -5.8 kg/s CO_2 abatement from heat production. Finally, based on SPECCA analysis, the CASOH-E demonstrates better technical performance with 2.2 $MJ_{LHV}/kg_{CO2,}$ followed by the CASOH-base case with 2.9 MJ_{LHV}/kg_{CO2}, and MDEA, with 3.1 MJ_{LHV}/kg_{CO2}.

Table 5. Technical comparison for the utility supply scenarios

		HY-GRID			HY-HY			NG-NG			NG-REN			REN-REN		
	No capture	**MDEA**	**CASOH-B**	**CASOH-E**	**MDEA**	**CASOH-B**	**CASOH-E**	**MDEA**	**CASOH-B**	**CASOH-E**	**MDEA**	**CASOH-B**	**CASOH-E**	**MDEA**	**CASOH-B**	**CASOH-E**
Thermal output [MW]	295.2	109	77.6	160.7	52.9	59.1	34.7	267	77.6	224.5	267	77.6	224.5	267	77.6	224.5
Cold gas efficiency [%]	100	36.9	26.3	54.4	17.9	20	11.8	90.6	26.3	76	90.6	26.3	76	90.6	26.3	76
Heat requirement [MW_{th}]	-	143	-46.0	57.4	143	-46	57.4	143	-46	57.4	143	-46	57.4	143	-46	57.4
Power requirement [MW_{el}]	-	33.6	11.1	75.6	33.6	11.1	75.6	33.6	11.1	75.6	33.6	11.1	75.6	33.6	11.1	75.6
Direct CO_2 emission [kg/s]	79.2	13.4	8.2	6.7	13.4	8.2	6.7	13.4	8.2	6.7	13.4	8.2	6.7	13.4	8.2	6.7
CO_2 emission by heat (indirect) [kg/s]	-	0	-5.8	0	0	-5.8	0	18.1	-5.8	7.3	18.1	-5.8	7.3	12	-4	4.8
CO_2 emission by electricity (indirect) [kg/s]	-	4.9	1.6	11.1	0	0	0	3.6	1.2	8	0.7	0.2	1.6	0.7	0.2	1.6
Total CO_2 emission [kg/s]	79.2	18.3	4	17.8	13.4	2.4	6.7	35.1	3.5	22	32.3	2.6	15.6	26.2	-3.6	13.2
Specific CO_2 emission [$kgCO_2/GJ_{LHV}$]	268.4	168	51.4	110.8	253	39.8	193	131	45.5	98	121	33.4	69.7	97.9	58.7	58.7
CCR [%]	-	76.8	95	77.5	83.1	97	91.5	55.7	95.5	72.3	59.3	96.7	80.3	67	94.2	83.4
SPECCA (direct) [$MJ_{LHV}/kgCO_2$]	-	2.8	3.1	1.9	3.7	3.3	3.6	0.4	3.1	1	0.4	3.1	1	0.4	3.1	1
SPECCA (total) [$MJ_{LHV}/kgCO_2$]	-	3.1	2.9	2.2	3.7	3.1	3.6	0.6	2.9	1.2	0.6	2.8	1.1	0.5	2.9	1.1

Scenario 2 (HY-HY): when compensating heat and electricity with the H_2-rich gas, notable impacts are observed on the MDEA and CASOH-E cases, leading to a reduction in the thermal output by 214.5 MW_{th} for MDEA and by 189.8 MW_{th} for CASOH-E. In contrast, the CASOH-B shows a relatively lower impact, decreasing the thermal output from 77.6 MW_{th} to 59.1 MW_{th}. Consequently, the CASOH-B achieves a higher cold gas efficiency of 20%, compared to 17.9% and 11.8% for MDEA and CASOH-E, respectively. Since the H_2-rich gas fully compensates for heat and electricity requirements, there is no additional associated CO_2 emission in these cases. Still, as in scenario (1), the 46.0 MW_{th} medium-grade recovered heat enables the CO_2 reduction of 5.8 kg/s CO_2 for the CASOH-B. Moreover, the CASOH-B performs better in CCR (97%) than the other cases. Despite having a lower thermal output compared to other cases, the CASOH-E showcases a competitive performance in terms of specific CO_2 emissions (193.0 kg_{CO2}/GJ_{LHV}) compared to MDEA and CASOH-B with 253.4 kg_{CO2}/GJ_{LHV} and 39.8 kg_{CO2}/GJ_{LHV}. The SPECCA analysis indicates that the CASOH-B with the SPECCA of 3.1 MJ_{LHV}/kg_{CO2} outperforms the other cases, which can be attributed to its higher thermal output.

Scenario 3 (NG-NG): In this scenario, heat and power requirements are provided from external sources using natural gas, which is state-of-the-art heat and power generation. As a result, there is no reduction in thermal output for any of the cases. The MDEA exhibits superior performance in terms of cold gas efficiency (90.6%) compared to the CASOH-B (26.3%) and the CASOH-E (76.0%). The additional emissions associated with utility requirements lead to specific CO_2 emissions of 45.5 kg_{CO2}/GJ_{LHV} for CASOH-B, 95.1 kg_{CO2}/GJ_{LHV} for CASOH-E, and 131.3 kg_{CO2}/GJ_{LHV} for MDEA. Moreover, the additional CO_2 from external sources reduced CCR, reaching 55.7% for MDEA and 72.3% for CASOH-E, compared to the previous values of 83.1% and 91.5% in scenario (2), respectively. The SPECCA analysis indicates that MDEA with a SPECCA of 0.6 MJ_{LHV}/kg_{CO2} performs significantly better when the energy requirement is provided externally from fossil-fuelled sources. Nonetheless, CASOH-E shows promising potential with a SPECCA of 1.2 MJ_{LHV}/kg_{CO2}.

Scenario 4 (NG-REN): When addressing energy needs from natural gas (heat) and photovoltaic energy (electricity), it's important to note that this setup does not affect thermal output in the cases examined. Consequently, MDEA appears as the front-runner regarding cold gas efficiency (90.6%). In contrast, CASOH-B and CASOH-E show 26.3% and 76.0% cold gas efficiencies, respectively. The additional emissions stemming from the operation of the natural gas boiler and the photovoltaic system contribute to an aggregate CO_2 emission load. The specific CO_2 emissions reach 33.4 kg_{CO2}/GJ_{LHV} for CASOH-B, 69.7 kg_{CO2}/GJ_{LHV} for CASOH-E, and 120.7 kg_{CO2}/GJ_{LHV} for MDEA. Furthermore, supplementary CO_2 emissions from the energy supplier lead to a reduction in CCR for MDEA (59.3%) and CASOH-E (80.3%). Notably, the CASOH-B shows a higher CCR (96.7%) due to negative CO_2

emissions associated with the additional heat being made available. Like scenario (3), the SPECCA metric reveals the superior performance of MDEA, achieving a SPECCA of 0.6 MJ_{LHV}/kg_{CO2} when relying on external energy sources.

Scenario 5 (REN-REN): In this scenario, where heat and power needs are met by external sources (a biogas-fuelled boiler and PV), the cold gas efficiency is 90.6% for MDEA, 26.3% for CASOH-B, and 76.0% for CASOH-E. CO_2 emissions from electricity generation remain consistent with scenario (4) due to the incorporation of PV technology. While the CASOH-B achieves a higher capture rate (94.2%) in comparison to the CASOH-E (83.4%), it's essential to note that the relatively lower thermal output of the CASOH-B results in a higher specific CO_2 emission (94.2 kg_{CO2}/GJ_{LHV}). In contrast, the CASOH-E exhibits a lower specific emission of 58.7 kg_{CO2}/GJ_{LHV}. Regarding the SPECCA, the MDEA case emerges as the top performer, with a SPECCA of 0.5 MJ_{LHV}/kg_{CO2}, while CASOH-E demonstrates a competitive performance with a SPECCA of 1.1 MJ_{LHV}/kg_{CO2}.

Overall, the previous evaluation revealed that choosing heat and power supply methods significantly impacts the technology's performance. Both CASOH-B and CASOH-E perform better in CO_2 capture efficiency than the MDEA (Figure 4). However, MDEA performs superior in certain scenarios, but its emissions can increase when relying on external energy sources. The comparison of SPECCA under the different scenarios for energy supply (Figure 5) reveals that MDEA outperforms the other cases when it relies on external heat and power sources. Moreover, it is worth mentioning that due to the heat recovery, CASOH-B performs better if it is close to a medium-grade heat consumer.

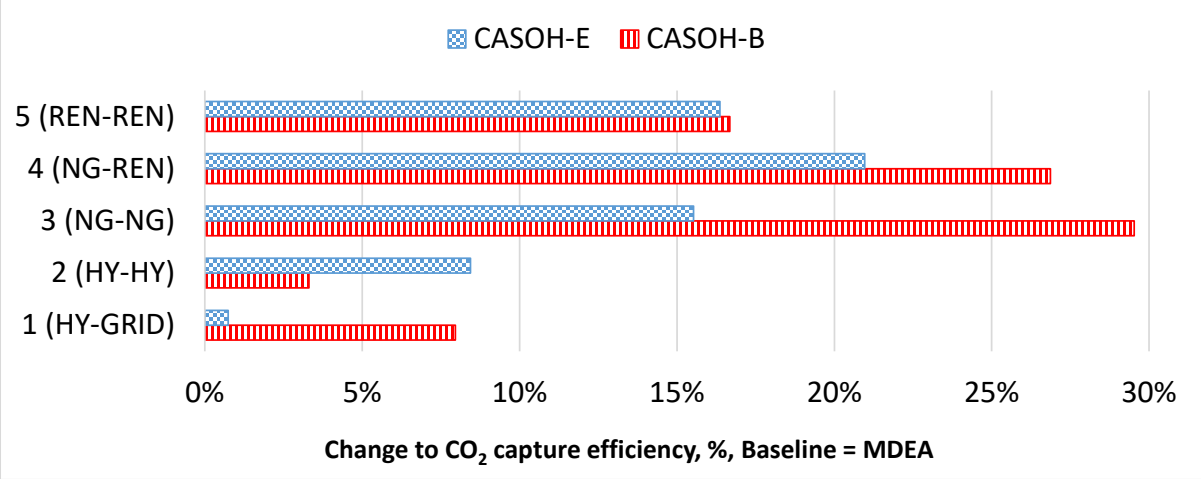

Figure 4. Change to CO_2 capture efficiency (%) under five energy supply scenarios. Baseline values for scenarios using MDEA capture

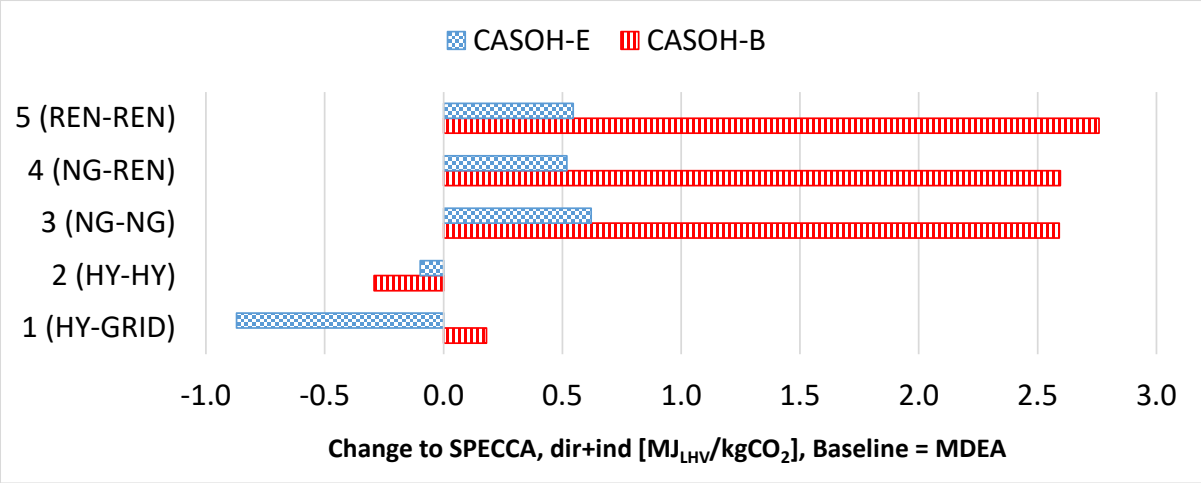

Figure 5. Change to SPECCA [$MJ_{LHV}/kgCO_2$] under five energy supply scenarios. Baseline values for scenarios using MDEA capture

3.3. Comparison of different CO_2 capture rates on CASOH-E

A sensitivity analysis was conducted on the CASOH-E case for different CO_2 capture rates. This is achieved by using only part of the BFG through the CASOH-E technology, hence reducing the size and footprint of the CO_2 capture plant. The separated fraction, the fraction of BFG bypassing the CASOH-E unit, is then mixed with the H_2-rich gas. Separated fractions of 5%, 10%, and 15% are considered in this analysis, and the results are detailed in Table 6.

Table 6. CASOH-E performance on different capture rates

		Split fraction			
	Unit	**0%**	**5%**	**10%**	**15%**
Total BFG Input	[MW_{LHV}]	295.2	295.2	295.2	295.2
Thermal energy output (DCF)	[MW_{LHV}]	224.5	228.0	231.5	235.1
Cold gas efficiency	[%]	76.0	77.2	78.4	79.6
Net power consumption	[MW_{el}]	75.2	72.3	71.3	68.4
Heat requirement	[MW_{th}]	57.4	54.5	53.6	52.7
CO_2 flow rate for storage	[kg/s]	72.6	68.9	65.3	61.7
CO_2 purity for storage	[%]	99.8	99.8	99.8	99.8
CO_2 capture efficiency	[%]	91.5	86.9	82.4	77.9
Specific CO_2 emission	[kg_{CO2}/GJ_{LHV}]	29.9	45.4	60.3	74.6

As the separated fraction (SF) of BFG to the CASOH-E plant is increased from 0% to 15%, some trends were observed, reflecting changes in system performance and efficiency. Thermal output rose from 224.5 MW_{LHV} to 235.1 MW_{LHV}, improving cold gas efficiency from 76.0% to 79.6%. Higher SF values reduced the amount of BFG entering the system, decreasing the need for compression work. This reduction was primarily driven by a decline in the flowrate of CO_2 for storage, which dropped from 72.6 kg/s to 61.7 kg/s. Additionally, the reduced BFG flow lowered the heat requirement due to

decreased steam production needs. However, specific emissions increased significantly from 29.9 kg_{CO2}/GJ_{LHV} to 74.6 kg_{CO2}/GJ_{LHV}, driven by a decline in the CO_2 capture rate from 91.5% to 77.9%.

3.4. Effect of calcination pressure on CASOH-E

A separate sensitivity analysis was conducted to evaluate the performance of CASOH-E under different calcination pressures. Reducing the calcination pressure reduces the steam demand to keep the same CO_2 partial pressure. Since CO_2 is taken at a lower pressure, more compression costs are envisaged to reach the target pressure for transportation and storage (110 bar).

Table 7 shows that increasing the calcination pressure from 0.5 to 1 bar increases the heat requirement from 57.4 to 158.6 MW_{th} because of the larger flowrate of H_2O required at the calcination stage. Other performance metrics, such as thermal energy output (224.5 MW_{LHV}), cold gas efficiency (76.0%), and CO_2 capture efficiency (91.5%), remain constant across all pressures. Similarly, the CO_2 flow rate for storage (72.5 kg/s) and CO_2 purity for storage (99.8%) are unaffected by changes in calcination pressure. Specific CO_2 emissions also remain steady at 29.8 kg_{CO2}/GJ_{LHV}, as the analysis does not account for additional emissions from heat and power compensation. These results suggest that while higher calcination pressures demand significantly more heat, they do not compromise the system's CO_2 capture or cold gas efficiency, maintaining stable performance in these areas. However, the increased heat requirement at higher pressures could affect overall energy efficiency and operational costs.

Table 7. CASOH-E performance at different calcination pressures

		Calcination pressure		
	Unit	**0.5 bar**	**0.75 bar**	**1 bar**
Total BFG Input	[MW_{LHV}]	295.2	295.2	295.2
Thermal energy output (DCF)	[MW_{LHV}]	224.5	224.5	224.5
Cold gas efficiency	[%]	76.0	76.0	76.0
Net power consumption	[MW_{el}]	75.2	71.5	68.4
Required heat	[MW_{th}]	57.4	113.1	158.6
CO_2 flow rate for storage	[kg/s]	72.5	72.5	72.5
CO_2 purity for storage	[%]	99.8	99.8	99.8
CO_2 emission	[kg/s]	6.7	6.7	6.7
CO_2 capture efficiency	[%]	91.5	91.5	91.5
Specific CO_2 emission	[kg_{CO2}/GJ_{LHV}]	29.8	29.8	29.8

It is worth mentioning that long-term operation of CASOH-based systems may be affected by degradation of CaO and CuO materials due to sintering, loss of surface area, and chemical deactivation. These effects can reduce sorbent reactivity and oxygen carrier stability over repeated cycles. Periodic reactivation or replacement of sorbents is typically required, as demonstrated in calcium looping pilot studies. While not explicitly modelled in this work, such operational

considerations are essential for future scale-up and are the focus of ongoing experimental activities within the project consortium.

4. Conclusions

This study provides a comprehensive technical comparison of blast furnace gas (BFG) decarbonisation using two configurations of the CASOH processes and the benchmark MDEA technology. Several key performance indicators were evaluated, considering different heat and power supply scenarios in the process. When heat and power were supplied externally, MDEA demonstrated superior thermal output and cold gas efficiency (267.4 MW_{LHV} and 90.6%) compared to the CASOH configurations, which ranged from 77.6 to 224.5 MW_{LHV} and 26.3% to 76%. Among the CASOH technologies, CASOH-B exhibited lower H_2-rich gas production than CASOH-E due to the regeneration strategies. When integrated with a downstream CO_2 purification unit (LT CO_2 partial condensation and/or (V)PSA), a variation of ±10% in the electricity requirement is noted with a variation in the CO_2 purity of ±1% by keeping the same recovery. However, CASOH-B achieved the highest CO_2 capture efficiency, outperforming both CASOH-E (71.2%–91.5%) and MDEA (53.2%–76.8%). In terms of energy efficiency, CASOH-E performed competitively with MDEA, achieving a specific energy consumption per carbon dioxide avoided (SPECCA) of 1.2–3.6 $MJ_{LHV}/kgCO_2$ compared to 0.5–3.7 MJ_{LHV}/kg_{CO2} for MDEA. Sensitivity analyses of CASOH-E revealed that increasing the split fraction, which diverts a portion of the BFG before entering the CASOH reactor, enhanced thermal output and cold gas efficiency while reducing compression work and heat requirements. However, this adjustment also increased specific CO_2 emissions due to a reduced capture rate. These findings highlight the potential for optimising BFG decarbonisation strategies by balancing thermal output, efficiency, and emissions capture. Further investigation of the economic and environmental performance of the CASOH technology for BFG decarbonisation and exploring the impact of operational parameters and energy prices is recommended for future studies.

Supporting Information: the detailed process flow diagrams and stream tables of the main plant configurations are supplied as Supporting Information.

Acknowledgements

The work was carried out as part of the European Union's Horizon 2020 research and innovation programme under grant agreement no. 884418 (C^4U project). The work reflects only the authors' views, and the European Union is not liable for any use that may be made of the information contained

therein. The authors would like to acknowledge the EPSRC for providing funding through the project BREINSTORM (Grant No. EP/S030654/1).

References

1. World Steel Association, *Sustainability Indicators Report*. 2023.
2. International Energy Agency, *Energy Technology Perspectives - Tracking Clean Energy Progress*. 2017.
3. Birat, J.-P., *Society, Materials, and the Environment: The Case of Steel.* Metals, 2020. **10**(3): p. 331.
4. Collis, J., et al., *Deriving Economic Potential and GHG Emissions of Steel Mill Gas for Chemical Industry.* Frontiers in Energy Research, 2021. **9**.
5. Kim, D. and J. Han, *Techno-economic and climate impact analysis of carbon utilization process for methanol production from blast furnace gas over Cu/ZnO/Al2O3 catalyst.* Energy, 2020. **198**: p. 117355.
6. Kim, C., et al., *Review of carbon dioxide utilization technologies and their potential for industrial application.* Journal of CO2 Utilization, 2022. **65**: p. 102239.
7. Fernández, J.R., V. Spallina, and J.C. Abanades, *Advanced Packed-Bed Ca-Cu Looping Process for the CO2 Capture From Steel Mill Off-Gases.* Frontiers in Energy Research, 2020. **8**.
8. Spallina, V., et al., *Chemical looping reforming in packed-bed reactors: Modelling, experimental validation and large-scale reactor design.* Fuel Processing Technology, 2017. **156**: p. 156-170.
9. Abbas, S.Z., et al., *Experimental assessment of reverse water gas shift integrated with chemical looping for low-carbon fuels.* Journal of CO2 Utilization, 2024. **83**: p. 102775.
10. Arias, B., et al., *Demonstration of steady state CO2 capture in a 1.7MWth calcium looping pilot.* International Journal of Greenhouse Gas Control, 2013. **18**: p. 237-245.
11. Samari, M., et al., *Direct capture of carbon dioxide from air via lime-based sorbents.* Mitigation and Adaptation Strategies for Global Change, 2020. **25**(1): p. 25-41.
12. Žalec, D., et al., *Process development and performance assessment of flexible calcium looping biomass gasification for production of renewable gas with adjustable composition.* International Journal of Energy Research, 2022. **46**(5): p. 6197-6215.
13. Masoudi Soltani, S., et al., *Sorption-enhanced Steam Methane Reforming for Combined CO2 Capture and Hydrogen Production: A State-of-the-Art Review.* Carbon Capture Science & Technology, 2021. **1**: p. 100003.
14. Yan, Y., et al., *Techno-economic analysis of low-carbon hydrogen production by sorption enhanced steam methane reforming (SE-SMR) processes.* Energy Conversion and Management, 2020. **226**: p. 113530.
15. Ströhle, J., et al., *Carbonate looping experiments in a 1MWth pilot plant and model validation.* Fuel, 2014. **127**: p. 13-22.
16. Astolfi, M., et al., *Calcium looping for power generation with CO2 capture: The potential of sorbent storage for improved economic performance and flexibility.* Applied Thermal Engineering, 2021. **194**: p. 117048.
17. Abanades, J.C., et al., *New CO2 Capture Process for Hydrogen Production Combining Ca and Cu Chemical Loops.* Environmental Science & Technology, 2010. **44**(17): p. 6901-6904.
18. Alarcón, J.M., J.R. Fernández, and J.C. Abanades, *Study of a Cu-CuO chemical loop for the calcination of CaCO3 in a fixed bed reactor.* Chemical Engineering Journal, 2017. **325**: p. 208-220.
19. Abbas, S.Z., et al., *A Ca-Cu Chemical Loop Process for CO2 Capture in Steel Mills: System Performance Analysis.* Proceedings of the 15th Greenhouse Gas Control Technologies Conference, 2021.

20. Abbas, S.Z., et al., *Lab-scale experimental demonstration of CaCu chemical looping for hydrogen production and in-situ CO2 capture from a steel-mill.* Fuel Processing Technology, 2022. **237**: p. 107475.
21. Khallaghi, N., et al. *D3.4 Parametric performance of the C4U technologies for the cluster optimization*. 2023; Available from: https://c4u-project.eu/wp-content/uploads/2024/08/C4U-D3.4-Parametric-performance-of-the-C4U-technologies_final.pdf.
22. Khallaghi N, et al., *Preliminary Techno-Economic Evaluation of Blast Furnace Gas Utilisation with Ca-Cu looping Cycle Integrated with CO2 Separation by Partial Condensation.* Proceedings of the 16th Greenhouse Gas Control Technologies Conference (GHGT-16) 23-24 Oct 2022, 2022.
23. Khallaghi, N., et al., *Techno-economic assessment of blast furnace gas pre-combustion decarbonisation integrated with the power generation.* Energy Conversion and Management, 2022. **255**: p. 115252.
24. EUROFER. *Map of EU steel production sites*. 2024; Available from: https://www.eurofer.eu/publications/brochures-booklets-and-factsheets/european-steel-in-figures-2024.
25. Grasa, G., et al., *Blast furnace gas decarbonisation through Calcium Assisted Steel-mill Off-gas Hydrogen production. Experimental and modelling approach.* Chemical Engineering Research and Design, 2023. **191**: p. 507-522.
26. Díaz, M., et al., *The Ca-Cu looping process using natural CO2 sorbents in a packed bed: Operation strategies to accommodate activity decay.* Chemical Engineering Science, 2023. **273**: p. 118659.
27. Fernandez, J.R., et al., *Decarbonization of Blast Furnace Gases Using a Packed Bed of Ca-Cu Solids in a New TRL7 Pilot.* Energies, 2025. **18**(3): p. 675.
28. Subraveti, S.G., et al., *Techno-economic assessment of optimised vacuum swing adsorption for post-combustion CO2 capture from steam-methane reformer flue gas.* Separation and Purification Technology, 2021. **256**: p. 117832.
29. Paul Noothout, et al. *CO_2 Pipeline Infrastructure*. 2013; Available from: https://ieaghg.org/publications/co2-pipeline-infrastructure/.
30. Guan, Z., et al., *Simulation and analysis of dual-reflux pressure swing adsorption using silica gel for blue coal gas initial separation.* International Journal of Hydrogen Energy, 2021. **46**(1): p. 683-696.
31. Allam RJ, White V., and John Miller, *Purification of carbon dioxide*. 2013: United States.
32. Hills, A.W.D., *The mechanism of the thermal decomposition of calcium carbonate.* Chemical Engineering Science, 1968. **23**(4): p. 297-320.
33. Masala, A., et al., *Conductive ZSM-5-Based Adsorbent for CO2 Capture: Active Phase vs Monolith.* Industrial & Engineering Chemistry Research, 2017. **56**(30): p. 8485-8498.
34. Argyris, P.A., et al., *Reducing the cost of low-carbon hydrogen production via emerging chemical looping process.* Energy Conversion and Management, 2023. **277**: p. 116581.
35. Ecoinvent. *Database 3.5*. 2019 Dec, 2020]; Available from: https://ecoinvent.org/the-ecoinvent-database/.
36. Ecoinvent Database 3.5. *Heat and power co-generation, biogas, gas engine, UK*. 2019 Jun, 2024]; Available from: https://ecoinvent.org/the-ecoinvent-database/.
37. Ecoinvent Database 3.5. *Electricity production, photovoltaic, 570kWp open ground installation, UK*. 2019 Jun, 2024]; Available from: https://ecoinvent.org/the-ecoinvent-database/.
38. Johnson, I., W.T. Choate, and A. Davidson, *Waste Heat Recovery. Technology and Opportunities in U.S. Industry*. 2008: United States. p. Medium: ED; Size: 112 p.

Blast furnace gas utilization with calcium-assisted steel mill off-gas hydrogen production (CASOH) technology: technical evaluation

Khallaghi, Navid

2025-07-23

Khallaghi N, Zapata-Boada S, Diaz Gutierrez M, et al., (2025) Blast furnace gas utilization with calcium-assisted steel mill off-gas hydrogen production (CASOH) technology: technical evaluation. Industrial & Engineering Chemistry Research, Volume 64, Issue 29, July 2025, pp. 14616-14627
https://doi.org/10.1021/acs.iecr.5c01422